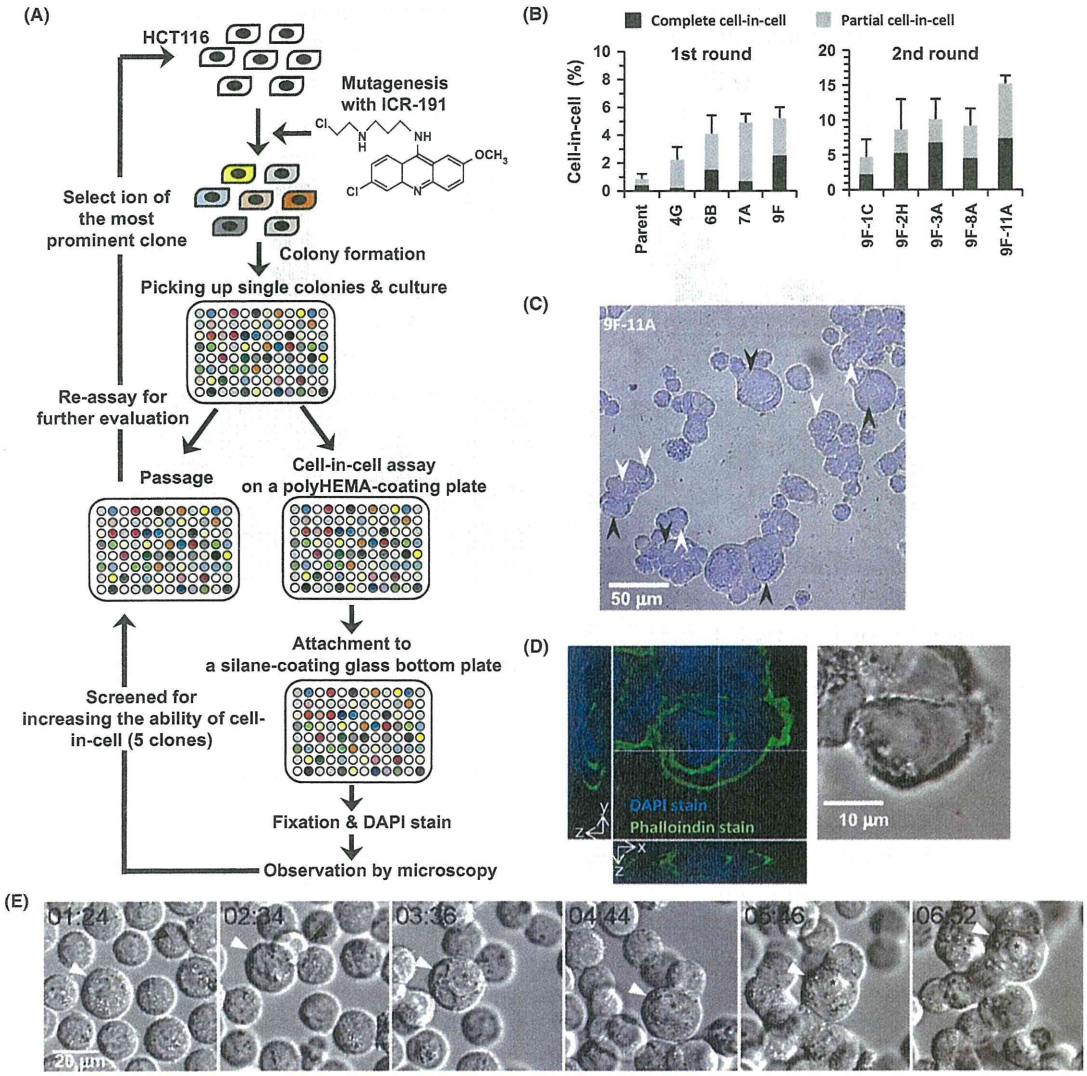

Figure 2 Establishment of a cell line showing enhanced formation of the cell-in-cell structures. (A) Screening of clones showing enhanced formation of cell-in-cell structures. HCT116 cells were exposed to 6.2 μg/mL of ICR-191, known as a frameshift mutagen, for 8 h. The culture medium was replaced with fresh medium, and the cells were recultured for 24 h. The cells were trypsinized and plated on ϕ100-mm dishes at a low density. After the colony formation, 144 single colonies were picked up, amplified and passaged on master and assay plates. The cells on the assay plate were transferred to a silane-coated glass-bottomed plate after culture for 14 h, centrifuged, fixed and stained with DAPI. Several clones were selected and furthermore evaluated. These mutagenesis/screening steps were repeated again. (B) The graph shows the results of the first and second round of screening. The clone 9F was used for the second round of screening. At least 1000 cells were counted. (C) Cell-in-cell structures of 9F-11A cells formed in the screening assay. DIC and DAPI fluorescence (blue) images of 9F-11A are merged. Black and white arrowheads indicate complete and partial cell-in-cell structures, respectively. (D) A whole image of a representative cell-in-cell structure. After fixation, cells were stained with DAPI (blue) and phalloidin–Alexa 488 (green). The right panel shows a light field. (E) Time-lapse imaging of internalization in the 9F-11A cells. DIC images were captured during cell culture on polyHEMA-coated glass-bottomed dishes at 2-min intervals. Black and white arrows show future internalized and host cells, respectively. The asterisk shows a completely internalized cell. Time zero corresponds to the initiation of the image capture immediately after plating of the cells on to a polyHEMA-coated glass-bottomed dish. The numbers of cells count in five experiments were as follows (cell-in-cell/total): 30/3372 (parent), 69/3329 (4G), 130/3344 (6B), 158/3257 (7A), 142/2757 (9F), 52/980 (9F-1C), 88/1084 (9F-2H), 60/678 (9F-3A), 105/1159 (9F-8A) and 186/1223 (9F-11A). Data represent the mean ± SD of the total rate of complete and partial cell-in-cell structures.

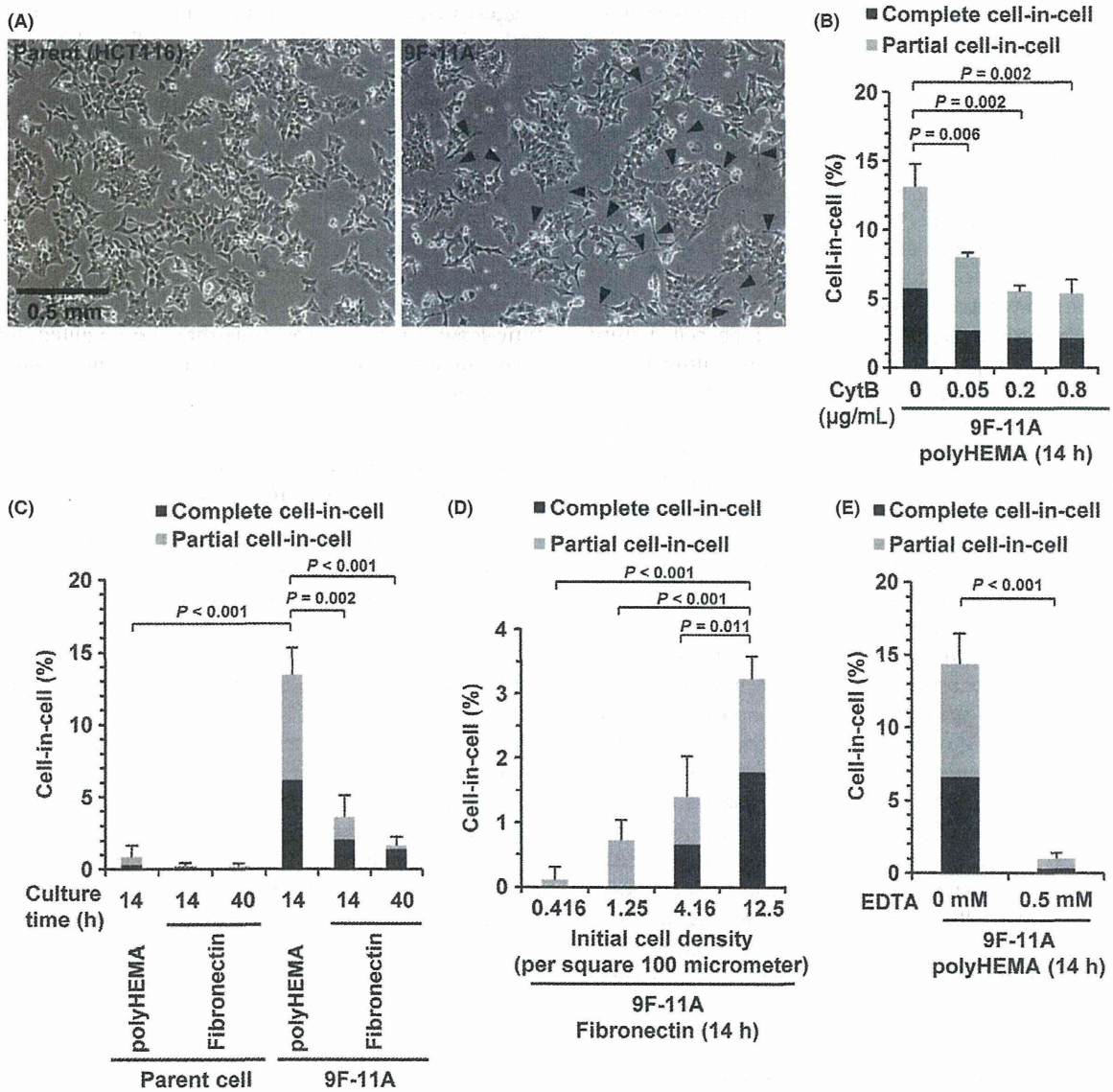

Figure 3 Culture conditions affecting the frequency of formation of cell-in-cell structures in 9F-11A. (A) Morphological differentiation between parent and 9F-11A cells. Parent (left) and 9F11-A (right) cells were subcultured under the cell-attachment condition. Arrows indicate representative slender pseudopodia. (B) Formation of cell-in-cell structures in the presence of cytochalasin B (CytB), an inhibitor of actin polymerization. 9F-11A cells were plated on polyHEMA-coated dishes in medium containing 0.05, 0.2 and 0.8 μg/mL of CytB. (C) Formation of cell-in-cell structures in the 9F-11A cells cultured on an adhesive-coated surface. Parent and 9F-11A cells were plated on fibronectin-coated and polyHEMA-coated dishes. (D) Formation of cell-in-cell structures in a cell density-dependent manner. 9F-11A cells were plated on fibronectin-coated dishes at the indicated cell densities and cultured for 14 h. (E) Suppression of the formation of cell-in-cell structures by EDTA chelation. 9F-11A cells were plated onto polyHEMA-coated dishes in medium containing 0.5 mM EDTA and cultured for 14 h. The numbers of cells count in three experiments were as follows (cell-in-cell/total): 152/1154 (CytB 0 μg/mL), 86/1074 (CytB 0.05 μg/mL), 67/1196 (CytB 0.2 μg/mL) and 58/1070 (CytB 0.8 μg/mL) in (B); 5/630 (parent polyHEMA), 3/1083 (parent fibronectin for 14 h), 3/1403 (parent fibronectin for 40 h), 89/690 (9F-11A-polyHEMA), 24/765 (9F-11A-fibronectin for 14 h) and 14/867 (9F-11A-fibronectin for 40 h) in (C); 1/566 (cell density 0.416), 4/566 (1.25), 8/539 (4.16) and 24/743 (12.5) in (D); and 90/625 (EDTA 0 mM) and 6/559 (0.5 mM) in (E). Data represent the mean ± SD of the total rate of complete and partial cell-in-cell structures.

cells under a little stimulation for the formation of cell-in-cell structures as possible. As expected, on the adhesive-coated dishes, the number of cell-in-cell structures in the 9F-11A cells decreased to less than one-fourth of that in the suspension culture condition (Fig. 3C; Student's *t*-test, $P < 0.001$ in the 9F-11A cells cultured on the adhesive-coated dishes for 40 h). Nonetheless, in the 9F-11A cells, the cell-in-cell structures occurred at a frequency of more than 1% on the adhesive-coated surface, being still higher than that for the parent cell line under the same condition. This was thought to be due to the high cell density (12.5 cells/100 μm^2) immediately after plating of the cells on the culture dishes, when the cells were still not attached to the bottom. The cell density of 12.5 cells/100 μm^2 corresponds to the cell crowdedness indicated in the first panel of Figure 2D, and frequent cell–cell contacts seemed to affect the formation of the cell-in-cell structures. In fact, the lower the culture cell density of the 9F-11A cells, the lower the number of cell-in-cell structures observed (Fig. 3D; Student's *t*-test, $P < 0.001$ in the cell density of 0.416 cells/100 μm^2). Furthermore, formation of the cell-in-cell structures in the 9F-11A cells was strongly suppressed in suspension culture condition even at the cell density of 12.5 cells/100 μm^2, by treatment with the chelating agent EDTA (ethylenediaminetetraacetic acid), which inhibits the formation of cell-in-cell structures (Overholtzer *et al.* 2007) (Fig. 3E; Student's *t*-test, $P < 0.001$). These results indicate that cell–cell contacts are indispensable for the formation of cell-in-cell structures and that plating at a low density on an adhesive-coated dish prevents the formation of the cell-in-cell structures to a great extent and is suitable for subculture of the 9F-11A cells.

Live cell behaviors of the internalized cells

In the cell-in-cell structures, the cells have been reported to remain alive after they are internalized (Lugini *et al.* 2006; Fais 2007; Overholtzer *et al.* 2007). Therefore, we focused on the behaviors of the internalized 9F-11A cells. Figure 4A and Movie S2 in Supporting Information show the time-lapse images of the internalization process of multiple cells (black arrowheads 1–3). Cell '1', which had been internalized by the host cell (white arrowhead), moved behind another internalized cell '2' and extruded out of the host cell simultaneously with the internalization of cell '3'. Furthermore, cell '1' divided into two daughter cells '1a' and '1b' immediately after emerging from the host cells. These scenes suggest that cell '1' was alive during both the entry and exit processes. In other cases, cells sinking into another cell sometimes showed pseudopodial dynamics in the process of formation of the cell-in-cell structures (Fig. 4B and Movies S3 and S4 in Supporting Information). The active pseudopodia were observed at the opposite side of the host cell, and the sinking cell seemed to be escaping from the host cell, or otherwise, thrashing toward the host cell. Although offense and defense between the outside and inside cells could not be elucidated from the time-lapse images, it was clear that the engulfed cells were still alive and active at least at the time of internalization.

Engulfment and invasion events in the cell-in-cell phenomenon observed in 9F-11A

The above results establish beyond doubt that the formation of cell-in-cell structures is promoted in the 9F-11A cells, but it still remained unclear which of the two processes, engulfment or invasion, was promoted because of the homotypic cell-in-cell event. Therefore, a labeling assay with fluorescent probes was carried out. HCT116 and 9F-11A cells were labeled with red and green fluorescent probes, respectively, and the cells were mixed, cultured in suspension condition and observed under a fluorescence microscope. As compared to the number of parent/parent (outside/inside) pairs, the number of the parent/9F-11A pairs was increased by approximately twofold (Fig. 5; Student's *t*-test, $P = 0.008$), as also that of the 9F-11A/9F-11A pairs (Student's *t*-test, $P = 0.006$). These results show that invasion events are increased by twofold in the 9F-11A cells as compared with that in the parent cells. Similarly, engulfment events were estimated to be increased by approximately fivefold in the 9F-11A cells as compared with that in the parent cells (Fig. 5; Student's *t*-test, $P < 0.001$ between parent/parent and 9F-11A/parent and between parent/9F-11A and 9F-11A/9F-11A). These results indicate that the events of both engulfment and invasion are activated in the 9F-11A cells and that 9F-11A cells show enhanced ability for both engulfment and invasion.

Discussion

Mutagenesis using ICR-191 has often been preferred to obtain cell clones of various phenotypes, such as resistance to virus infection (Bruce *et al.* 2005), aberrant cell replication (Zientek-Targosz *et al.* 2008) and

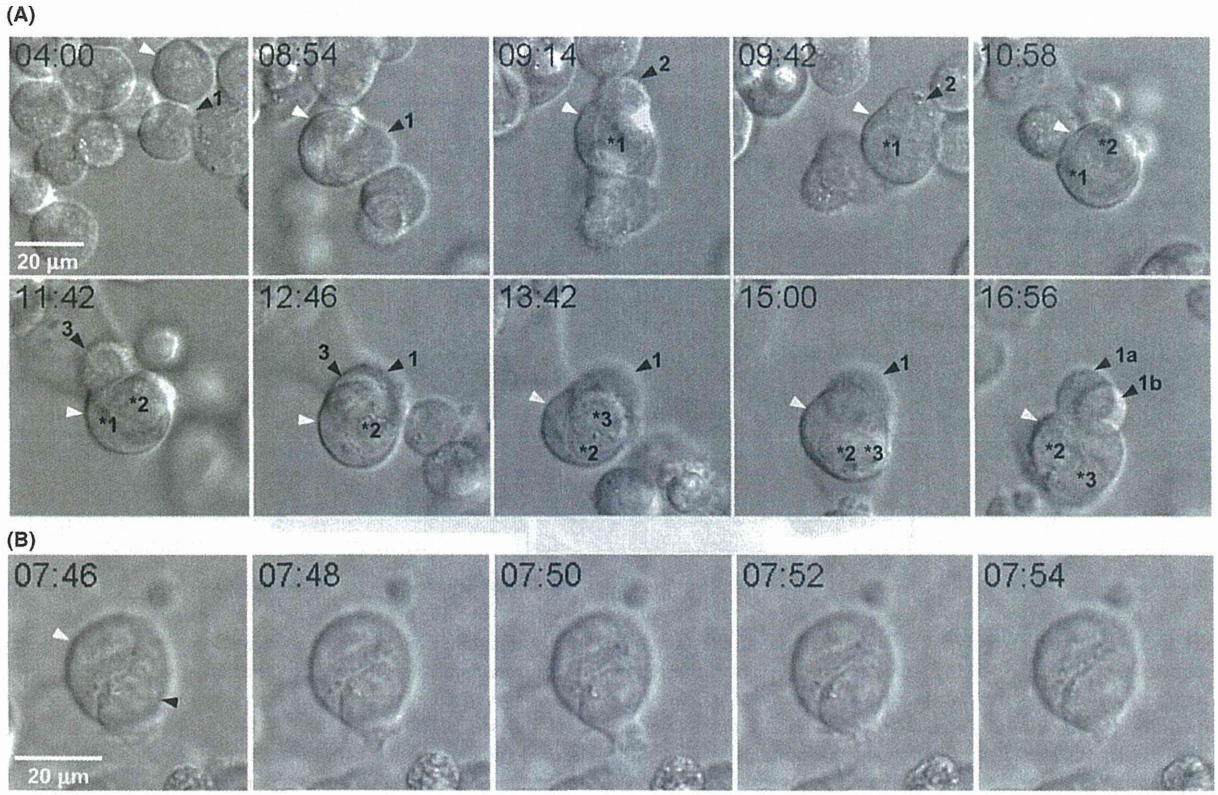

Figure 4 Live cell behaviors of the internalized cells. (A) Multiple cells (numbers 1–3) were internalized in the same host cell. Black and white arrows show future internalized and host cells, respectively. Arrow '1' cell divided into '1a' and '1b' cells immediately after emerging from the host cell. The asterisk shows a completely internalized cell. (B) Pseudopodial dynamics of a cell sinking into another cell. Time zero corresponds to the initiation of the image capture immediately after plating of the cells on a polyHEMA-coated glass-bottomed dish.

defective molecular signaling (Kohno *et al.* 2008). In this article, microscopic observation was used to screen cell clones showing enhanced formation of cell-in-cell structures. Cell-in-cell structures show remarkably varied appearances because of the dynamic cell behaviors, including partial and multiple internalizations. Therefore, there was no better method than using microscopic observational selection as a screening method to assay the cell-in-cell phenomenon. Another advantage of this method was that no second validation of the cell-in-cell structures was necessary due to the direct observation.

Although the mutagenized sites in the 9F-11A cells are soon expected to be identified through genomic analysis with a high-throughput DNA sequence, some putative molecules affected by mutagenesis can be presumed ahead of the genomic analysis. Active pseudopodia were observed during the process of formation of the cell-in-cell structures in the 9F-11A cells (Fig. 4B and Movies S3 and S4 in Supporting Information), and slender pseudopodia, which are rarely observed in the parent HCT116 cell line, were also often found under the cell-attachment culture condition (Fig. 3A). These findings suggest that the activities of actin regulatory proteins are aberrantly altered in the 9F-11A cells. Interestingly, several groups have reported that aberration of the actin polymerization pathway affects the frequency of formation of cell-in-cell structures: treatment with cytochalasin, an inhibitor of actin polymerization, suppressed active invasion of gastric carcinoma cells by the cytotoxic regulatory T-cell line HOZOT (Takeuchi *et al.* 2010); down-regulation of Rho-ROCK signaling led to a decrease in the cell invasion of MCF10A in suspension culture condition (Overholtzer *et al.* 2007); and expression of a deletion mutant form of ezrin, an actin-binding protein, reduced the cannibalistic activity of metastatic mela-

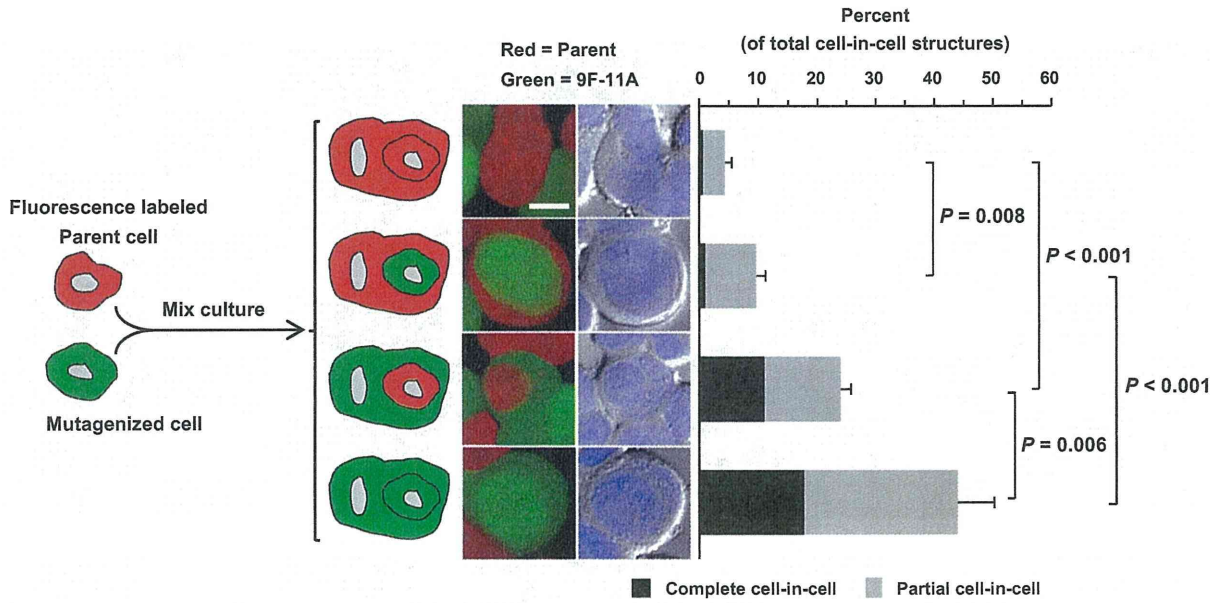

Figure 5 Increased ability of the 9F-11A cells for both engulfment and invasion involved in the formation of the cell-in-cell structures. Parent and 9F-11A cells were labeled with red and green fluorescent probes, respectively. The labeled cells were mixed, cultured in suspension condition and observed under a fluorescence microscope. The percent of cell-in-cell structures of each pair pattern per total number of cell-in-cell structures was represented. Fluorescence (left) and DIC (right) images are shown. Bar = 10 μm. The numbers of cell-in-cell structures in the three experiments were as follows: 13 (outside/inside = parent/parent), 30 (parent/9F-11A), 74 (9F-11A/parent) and 140 (9F-11A/9F-11A). Data represent the mean ± SD of the total rate of complete and partial cell-in-cell structures.

noma cells directed at live lymphocytes (Lugini *et al.* 2006). The treatment of cytochalasin actually suppressed the formation of the cell-in-cell structures in the mutagenized cells (Fig. 3B). The treatment of cells with ICR-191 is, if anything, thought to cause loss-of-function mutation because of the frameshift-biased mutation spectrum (Cariello *et al.* 1990). Therefore, it can be speculated that the actin-related molecules suppressing the formation of the protuberant structures such as pseudopodia observed in Fig. 3A and Fig. 4B were targeted by the mutagenesis, resulting in the enhanced formation of the cell-in-cell structures, although it cannot be ruled out that increased pseudopodia formation in the 9F-11A cells is not involved in the formation of the cell-in-cell structures.

Although the number of cell-in-cell structures was reduced in the cell-attachment condition, the suppressive mechanism is still not clear. Interestingly, complete cell-in-cell structures seemed to be more resistant to reduction in the cell-attachment condition than partial cell-in-cell structures (Figs. 1A and 3C). This could be due to the time lag between the formation of the cell-in-cell structures and attachment to the bottom. Once the cells are attached to the bottom, the cell-in-cell events are certain to be suppressed, and few partial features of cell-in-cell structures would be observed after the attachment. In contrast, if the cells were able to slowly advance from partial cell-in-cell structures formed during floating in the culture medium to complete cell-in-cell structures even after attachment to the bottom, it would be reasonable to expect a large number of complete cell-in-cell features on the adhesive coating than partial cell-in-cell structures. On the contrary, under the condition of low cell density, only partial cell-in-cell forms were observed on adhesive-coated dishes (Fig. 3C). This would be due to the delay in cell–cell contacts during floating. At a low cell density, engulfment and invasion are not likely to occur until just before the attachment to the bottom, because it takes a long time for cell–cell contacts to be established in a cell-sparse space. Thus, since there would be little time for the formation of cell-in-cell structures after the attachment to the bottom, no complete cell-in-cell forms are observed at a low cell density.

In previous reports, cell-in-cell-engaged cells seemed to prefer either one of the events of engulfment or invasion (Lugini *et al.* 2006; Takeuchi *et al.* 2010), and the ability of the cells to exhibit both in the formation of the cell-in-cell structures has never been discussed. In this article, we established a cell line that showed enhanced ability for both engulfment and invasion. This fact raises the question of what determines the cell fate, engulfment or invasion, in each 9F-11A cell. One of the clues to answering this question could be related to the heterogeneity of the cultured cells. Even if a single cell is cultured, the population of proliferating cells will show heterogeneity of the cell characteristics, such as the cell body size and transcriptional profiling (Dey-Guha *et al.* 2011; Narsinh *et al.* 2011). Thus, in 9F-11A, differences in the cellular characteristics from a contact partner cell, or differences in the cellular environment, may determine the alternative cell fate of engulfment or invasion, synergistically with the intracellular pathway affected by the mutagenesis. This hypothesis about the influence of the cellular environment can also be applied to other cell lines, including ones that show strong preference to either engulfment or invasion. Even a cell showing a prominent invasive phenotype must be stimulated for engulfment in some cellular environments, although an innate property for invasion may dominate over the stimulus for engulfment in most cases. The power balance between an innate property and stimulus from a cellular environment would determine which of engulfment and invasion occurs in each cell and also characterize the features of the cell-in-cell phenomenon in each cell line. Furthermore, our finding that both engulfment and invasion were increased in the mutagenized cell line shows that cell-in-cell structures can be formed not only by either process of enhanced engulfment or invasion, but also by both of these processes. This will be a key concept for understanding the physiological and pathological roles of cell-in-cell formation *in vivo*. Engulfment and invasion have been reported as different concepts and to be individually associated with specific biological roles, such as nutrient supply to the host cell in an engulfment event, and cell death of the host cell in an invasion event (Lugini *et al.* 2006; Takeuchi *et al.* 2010). The idea that cell-in-cell structures can be formed through a mixed process of enhanced engulfment and enhanced invasion may imply that cell-in-cell structures are not always homogeneously associated with either one of the biological roles and that there is the possibility that cell-in-cell structures have heterogeneous features mediating various biological roles.

Details of the cell-in-cell phenomenon have yet to be investigated considering that cell-in-cell structures have been reported for a long time. In this article, the ability of the cells to show both enhanced invasion and engulfment involved in the formation of cell-in-cell structures was showed through characterization of the mutagenized cell line. An understanding of this ability will be helpful in appreciating its biological events involved in the occurrence of the cell-in-cell phenomenon. In addition, genomic analysis of the mutagenized cell line may be expected to show the molecular mechanisms underlying the occurrence of the cell-in-cell phenomenon in future.

Experimental procedures

Cell culture and cell-in-cell assay

The human colorectal cancer cell line HCT116 (CCL-247; purchase date, 11/16/2005; American Type Culture Collection, Manassas, VA, USA), having a relatively stable karyotype, and the breast cancer cell line MCF7 (HTB-22; purchase date, 4/2/2013; American Type Culture Collection) were cultured at 37°C in RPMI medium (Life Technologies, Carlsbad, CA, USA) containing 10% fetal bovine serum (Nichirei, Tokyo, Japan) and penicillin–streptomycin solution (Life Technologies), under 5% CO_2. For the cell-in-cell assay, cultured cells (12.5 cells/100 μm^2) were plated on fibronectin (adhesive; Becton Dickinson, Franklin Lakes, NJ, USA)-coated glass slips (Kahyo *et al.* 2011) or polyHEMA (2-hydroxyethyl methacrylate; non-adhesive; Sigma–Aldrich)-coated dishes (Overholtzer *et al.* 2007) and cultured for 14 h. Cytochalasin B (final 0.05, 0.2 or 0.8 μg/mL; Sigma–Aldrich) and EDTA (final 0.5 or 2 mM; Sigma–Aldrich) were added to the medium at the start of culture. The cells on polyHEMA-coated dishes were transferred on silane (Sigma–Aldrich, St Louis, MO, USA)-coated glass slips and centrifuged at 33 × *g* for 5 min. In the screening experiment, silane-coated glass-bottomed 96-well plates were used instead of silane-coated glass slips. The cells were fixed with 4% paraformaldehyde (Sigma–Aldrich) at room temperature for 15 min and stained with DAPI (Life Technologies).

Mutagenesis and screening experiments

To acquire cell clones mutagenized with ICR-191, HCT116 cells were treated with 6.2 μg/mL of ICR-191 (dissolved in sterile distilled water, Sigma–Aldrich) for 8 h, cultured in fresh medium for 1 day, trypsinized and recultured at a low cell density (5000–10 000 cells/ϕ100-mm dish). The medium was exchanged with fresh medium once every 3 days, and 144 single cell colonies were picked up after culture for 9 days. The picked clone cells were passaged on 96-well plates (Thermo Scientific, Bremen, Germany), and each clone was distributed

into two plates for subculture and the cell-in-cell assay. In the case of the cell-in-cell assay, the cells were cultured at a high density on polyHEMA-coated plates, and the mutagenized cells were screened for cell-in-cell structures by differential interference contrast (DIC) optics and confocal laser scanning (FV1000; Olympus, Tokyo, Japan); then, four clones showing a relatively high frequency of cell-in-cell structures were selected, and cell counting showed that the 9F clone showed the largest number of cell-in-cell structures among the four clones. The 9F clone was amplified from the subculture plate and used for the second round of screening with ICR-191. Five clones with a relatively high frequency of cell-in-cell structures were selected of 144 single cell colonies from 9F clone, and the 9F-11A clone was finally evaluated as the cell clone showing cell-in-cell structures at the highest frequency. 9F-11A cells were subcultured at a low initial cell density (1 cell/100 μm^2) and used for the subsequent assays.

Microscopic analysis

When multiple cells were internalized by the same host cell, all the internalized cells were counted. In Fig. 2D, the fixed cells were stained with Alexa 488–phalloidin (Life Technologies) and observed using the *z*-stack imaging system (BZ-9000; Keyence, Osaka, Japan). For time-lapse imaging, the cells were plated on to polyHEMA-coated glass-bottomed dishes and cultured with the incubator microscope (FCV100; Olympus) for 20 h. DIC optical images were captured at 2-min intervals. To cover the visual field of the cells moving up and down, five capture steps were set up in a 20-μm *z*-axis range. In Fig. 3A, the images on the cell-attachment dishes (TPP, Trasadingen, Switzerland) were captured by the inverted microscope (Eclipse TS100; Nikon, Tokyo, Japan). Image data were analyzed by the Image J software (version 1.43f; National Institutes of Health, Bethesda, MD, USA).

Mixed culture assay using fluorescence probes

Parent cells and mutagenized cells (9F-11A) were cultured in medium containing 1 μM of CellTracker dye CMTMR (red fluorescence; Life technologies) and CMFDA (green fluorescence; Life technologies) for 30 min, respectively. Then, the medium was exchanged for fresh medium, and the cells were recultured for 30 min. After trypsinization, both the parent and mutagenized cells were washed with fresh medium, mixed with each other in equal amounts (final 12.5 cells/100 μm^2), plated on to polyHEMA-coated dishes and cultured for 14 h. Fluorescence images were captured by the confocal laser scanning system (FV1000).

Statistical analysis

The Student's *t*-test was used at the significance level of 0.05 (Figs. 1 and 3E) to statistically analyze the average rate of cell-in-cell structures. The Bonferroni correction was carried out for multiple comparison adjustment, in which the significance levels were 0.016 (Figs. 3B–D) and 0.012 (Fig. 5). The statistical analysis was carried out using the R software environment (R Core Team 2013). The rate of cell-in-cell structures was defined as the number of cell-in-cell structures per total number of cells (Figs. 1, 2 and 3) or as the number of cell-in-cell structures of each pair pattern per total number of cell-in-cell structures (Fig. 5).

Acknowledgements

This work was supported by grants from the Takeda Science Foundation; Grants-in-Aid for the U.S.–Japan Cooperative Medical Science Program; the National Cancer Center Research and Development Fund; Grants-in-Aid for Young Scientists (B) from the Japan Society for the Promotion of Science [grant number 23790396]; Priority Areas from the Japanese Ministry of Education, Culture, Sports, Science and Technology [20014007, 22659072, 221S0001]; and Grants-in-Aid for Cancer Research from the Japanese Ministry of Health [23120201 and 10103838].

References

Bauchwitz, M.A. (1981) The bird's eye cell: cannibalism or abnormal division of tumor cells. *Acta Cytol.* **25**, 92.

Brouwer, M., de Ley, L., Feltkamp, C.A., Elema, J. & Jongsma, A.P. (1984) Serum-dependent "cannibalism" and autodestruction in cultures of human small cell carcinoma of the lung. *Cancer Res.* **44**, 2947–2951.

Bruce, J.W., Bradley, K.A., Ahlquist, P. & Young, J.A. (2005) Isolation of cell lines that show novel, murine leukemia virus-specific blocks to early steps of retroviral replication. *J. Virol.* **79**, 12969–12978.

Cariello, N.F., Keohavong, P., Kat, A.G. & Thilly, W.G. (1990) Molecular analysis of complex human cell populations: mutational spectra of MNNG and ICR-191. *Mutat. Res.* **231**, 165–176.

Dey-Guha, I., Wolfer, A., Yeh, A.C., G Albeck, J., Darp, R., Leon, E., Wulfkuhle, J., Petricoin, E.F. 3rd, Wittner, B.S. & Ramaswamy, S. (2011) Asymmetric cancer cell division regulated by AKT. *Proc. Natl Acad. Sci. USA* **108**, 12845–12850.

Fais, S. (2007) Cannibalism: a way to feed on metastatic tumors. *Cancer Lett.* **258**, 155–164.

Florey, O., Kim, S.E., Sandoval, C.P., Haynes, C.M. & Overholtzer, M. (2011) Autophagy machinery mediates macroendocytic processing and entotic cell death by targeting single membranes. *Nat. Cell Biol.* **13**, 1335–1343.

Humble, J.G., Jayne, W.H. & Pulvertaft, R.J. (1956) Biological interaction between lymphocytes and other cells. *Br. J. Haematol.* **2**, 283–294.

Iyer, V.K., Handa, K.K. & Sharma, M.C. (2009) Variable extent of emperipolesis in the evolution of Rosai Dorfman disease: Diagnostic and pathogenetic implications. *J. Cytol.* **26**, 111–116.

Kahyo, T., Iwaizumi, M., Shinmura, K., Matsuura, S., Nakamura, T., Watanabe, Y., Yamada, H. & Sugimura, H. (2011) A novel tumor-derived SGOL1 variant causes abnormal mitosis and unstable chromatid cohesion. *Oncogene* **30**, 4453–4463.

Kohno, T., Daa, T., Otani, H., Shimokawa, I., Yokoyama, S. & Matsuyama, T. (2008) Aberrant expression of BAFF receptor, a member of the tumor necrosis factor receptor family, in malignant cells of nonhematopoietic origins. *Genes Cells* **13**, 1061–1073.

Krajcovic, M., Johnson, N.B., Sun, Q., Normand, G., Hoover, N., Yao, E., Richardson, A.L., King, R.W., Cibas, E.S., Schnitt, S.J., Brugge, J.S. & Overholtzer, M. (2011) A non-genetic route to aneuploidy in human cancers. *Nat. Cell Biol.* **13**, 324–330.

Krysko, D.V. & Vandenabeele, P. (2010) Clearance of dead cells: mechanisms, immune responses and implication in the development of diseases. *Apoptosis* **15**, 995–997.

Lee, K.P. (1989) Emperipolesis of hematopoietic cells within megakaryocytes in bone marrow of the rat. *Vet. Pathol.* **26**, 473–478.

Lugini, L., Matarrese, P., Tinari, A., Lozupone, F., Federici, C., Iessi, E., Gentile, M., Luciani, F., Parmiani, G., Rivoltini, L., Malorni, W. & Fais, S. (2006) Cannibalism of live lymphocytes by human metastatic but not primary melanoma cells. *Cancer Res.* **66**, 3629–3638.

Martinez, M., Samms, M., Hendrix, T.M., Adeosun, O., Pezzano, M. & Guyden, J.C. (2007) Thymic nurse cell multicellular complexes in HY-TCR transgenic mice demonstrate their association with MHC restriction. *Exp. Biol. Med. (Maywood)* **232**, 780–788.

Narsinh, K.H., Sun, N., Sanchez-Freire, V., Lee, A.S., Almeida, P., Hu, S., Jan, T., Wilson, K.D., Leong, D., Rosenberg, J., Yao, M., Robbins, R.C. & Wu, J.C. (2011) Single cell transcriptional profiling reveals heterogeneity of human induced pluripotent stem cells. *J. Clin. Invest.* **121**, 1217–1221.

Overholtzer, M. & Brugge, J.S. (2008) The cell biology of cell-in-cell structures. *Nat. Rev. Mol. Cell Biol.* **9**, 796–809.

Overholtzer, M., Mailleux, A.A., Mouneimne, G., Normand, G., Schnitt, S.J., King, R.W., Cibas, E.S. & Brugge, J.S. (2007) A nonapoptotic cell death process, entosis, that occurs by cell-in-cell invasion. *Cell* **131**, 966–979.

R Core Team (2013) *R: A Language and Environment for Statistical Computing*. R Foundation for Statistical Computing, Vienna, Austria. http://www.R-project.org/

Ritter, M.A., Sauvage, C.A. & Cotmore, S.F. (1981) The human thymus microenvironment: in vivo identification of thymic nurse cells and other antigenically-distinct subpopulations of epithelial cells. *Immunology* **44**, 439–446.

Schmitt, A., Jouault, H., Guichard, J., Wendling, F., Drouin, A. & Cramer, E.M. (2000) Pathologic interaction between megakaryocytes and polymorphonuclear leukocytes in myelofibrosis. *Blood* **96**, 1342–1347.

Sharma, N. & Dey, P. (2011) Cell cannibalism and cancer. *Diagn. Cytopathol.* **39**, 229–233.

Steinhaus, J. (1981) Ueber carcinoma-einschlusse. *Virchows Arch.* **126**, 533–535.

Takeda, K. & Akira, S. (2001) Roles of Toll-like receptors in innate immune responses. *Genes Cells* **6**, 733–742.

Takeuchi, M., Inoue, T., Otani, T., Yamasaki, F., Nakamura, S. & Kibata, M. (2010) Cell-in-cell structures formed between human cancer cell lines and the cytotoxic regulatory T-cell line HOZOT. *J. Mol. Cell Biol.* **2**, 139–151.

Wekerle, H. & Ketelsen, U.P. (1980) Thymic nurse cells–Ia-bearing epithelium involved in T-lymphocyte differentiation? *Nature* **283**, 402–404.

Woulfe, D.S., Lilliendahl, J.K., August, S., Rauova, L., Kowalska, M.A., Abrink, M., Pejler, G., White, J.G. & Schick, B.P. (2008) Serglycin proteoglycan deletion induces defects in platelet aggregation and thrombus formation in mice. *Blood* **111**, 3458–3467.

Zientek-Targosz, H., Kunnev, D., Hawthorn, L., Venkov, M., Matsui, S., Cheney, R.T. & Ionov, Y. (2008) Transformation of MCF-10A cells by random mutagenesis with frameshift mutagen ICR191: a model for identifying candidate breast-tumor suppressors. *Mol. Cancer* **7**, 51.

Received: 30 January 2013
Accepted: 13 August 2013

Supporting Information

Additional Supporting Information may be found in the online version of this article at the publisher's web site:

Figure S1 Growth sensitivity of HCT116 to ICR-191. HCT116 cells were treated with ICR-191 (final 2, 5 or 10 μg/mL) for 8 h, and cultured with fresh medium for 1 day. Cell counting was performed using the Cell Counting Kit (Dojindo, Kumamoto, Japan), and the cells showed 50% survival around 6.2 μg/mL of ICR-191.

Movie S1 A representative cell-in-cell process in 9F-11A. This movie corresponds to the montage images shown in Fig. 2E. Bar = 20 μm.

Movie S2 Internalization process of multiple cells in 9F-11A. This movie corresponds to the montage images shown in Fig. 4A. Bar = 20 μm.

Movie S3 Pseudopodial dynamics during the process of appearance of cell-in-cell structures in 9F-11A. This movie corresponds to the montage images shown in Fig. 4B. Bar = 20 μm.

Movie S4 Pseudopodial dynamics during the process of appearance of cell-in-cell structures in 9F-11A. Bar = 20 μm.

Journal of Surgical Oncology 2014;109:189–197

TNK2 Gene Amplification is a Novel Predictor of a Poor Prognosis in Patients With Gastric Cancer

KAZUYA SHINMURA, MD, PhD,[1]* SHINICHIRO KIYOSE, BS,[1] KIYOKO NAGURA, BS,[1] HISAKI IGARASHI, BS,[1] YUSUKE INOUE, MD,[1] SATOKI NAKAMURA, MD, PhD,[1] MATSUYOSHI MAEDA, MD, PhD,[2] MEGUMI BABA, MD, PhD,[3] HIROYUKI KONNO, MD, PhD,[3] AND HARUHIKO SUGIMURA, MD, PhD[1]

[1]*Department of Tumor Pathology, Hamamatsu University School of Medicine, Hamamatsu, Japan*
[2]*Department of Pathology, Toyohashi Municipal Hospital, Toyohashi, Japan*
[3]*Department of Surgery 2, Hamamatsu University School of Medicine, Hamamatsu, Japan*

Backgrounds and Objectives: We previously examined the amplification status of 10 kinase genes (*PIK3CA*, *EPHB3*, *TNK2*, *PTK7*, *EGFR*, *MET*, *ERBB2*, *HCK*, *SRC*, and *AURKA*) in gastric cancer (GC). This study aimed to determine the prognostic significance of these gene amplifications in GC.
Methods: A survival analysis was performed for GC patients. Since *TNK2* amplification was identified as a prognostic marker in the analysis, we also examined the functional effect of TNK2 overexpression on gastric cells.
Results: A Kaplan–Meier analysis showed that the prognosis of patients with GC exhibiting *TNK2* or *AURKA* amplification was significantly poorer than the prognosis of patients with GC without *TNK2* or *AURKA* amplification. A further multivariate analysis revealed that *TNK2* amplification was an independent predictor of a poor survival outcome among patients with GC (hazard ratio, 3.668; 95% confidence interval, 1.513–7.968; $P = 0.0056$). TNK2-overexpressing GC cells showed an increase in cell migration and non-anchored cell growth. Finally, microarray and pathway analyses revealed the aberrant regulation of some cancer-related pathways in TNK2-overexpressing GC cells.
Conclusions: These results suggested that *TNK2* amplification is an independent predictor of a poor prognosis in patients with GC and leads to an increase in the malignant potential of GC cells.
J. Surg. Oncol. 2014;109:189–197.

KEY WORDS: **gastric cancer; gene amplification; prognostic marker; survival analysis; TNK2**

INTRODUCTION

TNK2 (also known as Ack1) is a non-receptor tyrosine kinase consisting of a sterile α-motif domain, a tyrosine kinase domain, an SH3 domain, a Cdc42/Rac interactive binding domain, proline-rich sequences, and an ubiquitin association domain [1,2]. TNK2 is ubiquitously expressed in humans [3] and senses extracellular signals by interacting with membrane-bound activated receptor-tyrosine kinases such as EGFR, HER2, ALK, and MERTK [3–6]. Such interactions result in not only TNK2 activation, but also signal transduction through the activation of various downstream effector proteins, such as Cdc42, AKT, androgen receptor (AR), and Wwox [1,4,7–9]. Through these TNK2-signaling networks, TNK2 participates in survival, migration, and tumorigenesis [2].

The *TNK2* gene is amplified in various human carcinomas including lung, ovarian, gastric, and prostate cancer, and *TNK2* gene amplification leads to an elevated mRNA transcript level [10,11]. TNK2 overexpression causes increases in metastasis and mortality in a mouse model, and TNK2 is involved in an extracellular matrix-induced integrin signal, resulting in the activation of signaling processes such as the activation of the small GTPase Rac [10]. However, whether *TNK2* amplification is a prognostic factor in human cancer has not yet been reported.

We recently examined the amplification status of 100 kinase genes using a fluorescence in situ hybridization (FISH) analysis with a tissue microarray (TMA) containing a total of 60 carcinomas, consisting of colorectal, lung, and gastric carcinomas [11]. We then selected 10 kinases (*PIK3CA*, *EPHB3*, *TNK2*, *PTK7*, *EGFR*, *MET*, *ERBB2*, *HCK*, *SRC*, and *AURKA*) for which genomic amplification was detected at a frequency of 5% or more and examined the amplification status of these genes in more than 300 gastric cancers (GCs) [12]. Since gene amplification in cancer can sometimes define the prognosis of cancer patients [13–16], in the present study, we tested whether the amplification of the 10 above-mentioned genes was capable of predicting the prognosis of patients with GC and found that *TNK2* amplification independently predicts a poor survival among patients with GC. Then, to investigate the underlying mechanism, we also examined the effect of TNK2 overexpression on gastric cells.

Abbreviations: BAC, bacterial artificial chromosome; FISH, fluorescence in situ hybridization; GC, gastric cancer; TMA, tissue microarray.

Grant sponsor: Ministry of Health, Labour and Welfare;
Grant number: 21-1; Grant sponsor: Japan Society for the Promotion of Science;
Grant number: 25460476; Grant sponsor: Ministry of Education, Culture, Sports, Science and Technology;
Grant number: 221S0001

*Correspondence to: Kazuya Shinmura, MD, PhD, Department of Tumor Pathology, Hamamatsu University School of Medicine, 1-20-1 Handayama, Higashi Ward, Hamamatsu, Shizuoka 431-3192, Japan. Fax: +81-53-435-2225. E-mail: kzshinmu@hama-med.ac.jp

Received 31 July 2013; Accepted 10 October 2013

DOI 10.1002/jso.23482

Published online 31 October 2013 in Wiley Online Library (wileyonlinelibrary.com).

MATERIALS AND METHODS

Cell Line and Primary Carcinomas

A GC cell line AGS was obtained from the American Type Culture Collection (Manassas, VA). The AGS cells and their derivatives were maintained at 37°C in RPMI1640 medium supplemented with 10% fetal bovine serum (Equitech-Bio, Kerrville, TX) and penicillin/streptomycin under a 5% CO_2 atmosphere. GC tissues from two groups of primary GC patients (n = 271 and n = 335) were obtained from the Toyohashi Municipal Hospital (Japan) and the Hamamatsu University Hospital (Japan), respectively. The study design was approved by the institutional review board.

Preparation of TMA Blocks

A TMA block was prepared by transferring a cylinder with a diameter of 3 mm from each paraffin-embedded tissue sample using a microarrayer (KIN-1; Azumaya, Tokyo, Japan). The histopathological diagnosis of gastric cancer was confirmed by three pathologists (K.S., M.M., and H.S.).

FISH Analysis

TMA sections were de-waxed and re-hydrated, then boiled in 0.01 M citrate buffer (pH 6.0) to release the closed chromosomal structures. A combination of Cy3-labeled bacterial artificial chromosome (BAC) clone (RP11-436M6) for the *TNK2* locus (Advanced GenoTechs Co., Tsukuba, Japan) and a Spectrum Green-labeled control probe for the near centromere locus on chromosome 3 (BAC clone: RP11-91A15) or a combination of Cy3-labeled BAC clone (RP11-65K20) for the *AURKA* locus (Advanced GenoTechs Co.) and a Spectrum Green-labeled control probe for the near centromere locus on chromosome 20 (BAC clone: RP11-32N12) were placed on a slide and covered with a coverslip. The slides with the hybridization mixture were denatured on a digital hot plate (HP-15; AS ONE Corp., Osaka, Japan) and then incubated overnight at 42°C. After washing the slide in 50% formamide/2X SSC, mounting medium containing DAPI (Vector Laboratories, Burlingame, CA) was used for nuclear counterstaining. The slides were promptly examined under a fluorescence microscope (Olympus BX-51-FL; Olympus, Tokyo, Japan) equipped with epifluorescence filters and a photometric CCD camera (Sensicam; PCO Company, Kelheim, Germany). The images captured were digitized and stored in the image analysis program (MetaMorph; Molecular Devices, Palo Alto, CA). The average ratio of the TNK2 or AURKA signal number to the control probe signal number was calculated for each cancer. If the ratio of a cancer was >2.2, the cancer was defined as *TNK2* or *AURKA* amplification-positive.

Immunohistochemical Analysis

TMA sections were used for immunohistochemical staining using a Histofine Simple Stain MAX PO kit (Nichirei, Tokyo, Japan), as described previously [17]. An anti-phospho-TNK2 (Tyr284) (Millipore, Billerica, MA) was used as a primary antibody. Immunohistochemical signals were scored into three grades according to the intensity of staining: 0, 1+, and 2+. The percentages of positive cells were also scored into four categories: 0 (0%), 1+ (1–33%), 2+ (34–66%), and 3+ (67–100%). The products of the intensity and the percentage scores were used as a staining score.

Expression Plasmids

The pXJ-HA-ACK1 expression vector [7] and the FLAG-ACK1 expression vector [18] were kind gifts from Dr. Edward Manser (A-Star Neuroscience Research Partnership, Singapore) and Dr. W. Todd Miller (Stony Brook University, USA), respectively. The human *TNK2* cDNA was amplified using a polymerase chain reaction (PCR) with *PfuUltra* Hotstart DNA polymerase (Stratagene, La Jolla, CA) and the pXJ-HA-ACK1 expression vector [7] as a template; the amplified sequence was then inserted into a piggyBac cumate switch inducible vector (System Biosciences, Mountain View, CA) at the *Nhe*I and *Not*I restriction enzyme sites. The vector sequence was confirmed using DNA sequencing with a BigDye Terminator Cycle Sequencing Reaction Kit (Applied Biosystems, Tokyo, Japan) and an ABI 3100 Genetic Analyzer (Applied Biosystems).

Establishment of Stable Inducible Cell Lines

AGS cells were transfected with the piggyBac cumate switch inducible vector for TNK2 expression together with the piggyBac transposase vector (System Biosciences). To establish stable inducible cell lines, positively transposed cells were selected using puromycin (1.1 μg/ml). Since the inducible piggyBac vector features a tight cumate switch combined with an EF1-CymR repressor-T2A-Puro cassette to establish stable cell lines, the addition of cumate solution (System Biosciences) to the puromycin-selected cells leads to the induction of TNK2 expression.

Western Blot Analysis

A Western blot analysis using an anti-TNK2 polyclonal antibody (Sigma–Aldrich, St. Louis, MO) or an anti-β-tubulin monoclonal antibody (clone 2-28-33; Sigma-Aldrich) was performed as described previously [19].

Indirect Immunofluorescence Analysis

Cells were fixed with 4% paraformaldehyde, blocked with 10% normal goat serum, and probed with rabbit anti-TNK2 polyclonal antibody (Sigma–Aldrich), mouse anti-HA monoclonal antibody (16B12; Covance, Berkeley, CA), or mouse anti-FLAG monoclonal antibody (M2; Sigma–Aldrich). Indirect immunofluorescence labeling was performed by exposure to an Alexa Fluor 546 or 594-conjugated secondary antibody (Molecular Probes, Eugene, OR), and the nuclei were stained with 4′,6-diamidino-2-phenylindole (DAPI) (Sigma–Aldrich) [17]. Fluorescence signals were detected and stored as described in the "FISH analysis" section.

Transwell Migration Assay

The migration assay was performed using a six-well plate with an 8.0-μm pore polycarbonate membrane insert (Coring, Lowell, MA). The cells were seeded in the top chamber of the plate containing the transwell insert and were allowed to migrate for 24 hr at 37°C. Afterwards, the number of cells that had migrated to the bottom compartment was counted using a hemocytometer.

Non-Anchored Growth Assay

Cells were seeded in a 24-well ultra low attachment plate (Corning) and the plate was incubated at 37°C for 4 days. The number of cells growing in the media was counted using a hemocytometer.

Microarray Analysis and Mappfinder Analysis

Human gene expression was examined using the GeneChip Human Gene 1.0 ST array (Affymetrix, Santa Clara, CA). The Human Gene 1.0 ST array is comprised of 764,885 unique 25-mer oligonucleotide probes, constituting 28,869 gene probe sets. The total RNA was extracted using